# Correlation between Antigen-Combining-Site Structures and Functions within a Panel of Catalytic Antibodies Generated against a Single Transition State Analog

**Ikuo Fujii,* Fujie Tanaka, Hideaki Miyashita, Ryuji Tanimura, and Keiko Kinoshita**

*Contribution from the Protein Engineering Research Institute, 6-2-3 Furuedai, Suita, Osaka 565, Japan*

*Received December 29, 1994*[⊗]

**Abstract:** The diversity of the immune response, which can provide a panel of catalytic antibodies with varying degrees of catalytic activity and substrate specificity by immunization with a single hapten, raises the question concerning the extent to which a rationally designed hapten dictates the paratopes for catalytic function in the antigen-combining site. We have investigated the biochemical properties within a panel of six hydrolytic catalytic antibodies elicited against a phosphonate transition state analog **3** and have examined the correlation between the functions and the antigen-combining-site structures. Although the individual values for $k_{cat}$, $K_m$, and $K_{TSA}$ (the affinity for the transition state analog) of the six antibodies differed substantially, the transition state analysis ($k_{cat}/k_{uncat}$ versus $K_S/K_{TSA}$) displayed a linear relationship (slope = 0.99) with the four antibodies 6D9, 8D11, 4D5, and 9C10, which have homologous primary amino acid sequences, providing evidence that all of the differential binding energy of the transition state vs the ground state is available for the rate enhancement. This also suggested that these four antibodies catalyze the hydrolysis by variations of the same basic mechanism of transition state stabilization. In antibody 6D9, the difference in free energy between the antibody-catalyzed and uncatalyzed reactions was calculated to be 4.0 kcal/mol, a value that is consistent with the typical binding energy for one hydrogen bond between charged and uncharged groups in enzyme–substrate complexes. On the other hand, antibody 7C8, which has an amino acid sequence different from those of the others, deviated from the linear relationship observed in the transition state analysis, suggesting that catalytic factors other than transition state stabilization, such as a functioning acid or base, are involved in the catalysis. Thus, the difference in the catalytic properties is reflected in the differences in the Fv amino acid sequences. The analysis of the substrate specificity suggested that the catalytic antibodies with highly homologous primary amino acid sequences possess homogeneous binding modes to the substrate or hapten. The three-dimensional molecular model of the antibody 6D9–hapten complex reveals that the phosphonate moiety in the hapten interacts with His (L27d), a catalytic amino acid residue participating in the transition state stabilization in the antibody-catalyzed reactions. This histidine is conserved in the catalytic antibodies 6D9, 8D11, 4B5, and 9C10, and chemical modification by DEPC treatment caused a complete loss of the hydrolytic activity. Although the amino acid sequence of antibody 3G6 is highly homologous to the other four catalytic antibodies, antibody 3G6 has Tyr (L27d), which had reduced activity when modified with tetranitromethane. It is noteworthy that the majority of these catalytic antibodies, generated against a single transition state analog, display high homology in the biochemical and structural properties and catalyze the reaction with the same mechanism expected from designing the transition state analog. These findings emphasize the critical importance of hapten affinity to transition state stabilization and of chemically designing haptens that closely resemble the true transition state for the generation of catalytic antibodies.

## Introduction

Since the diversity of the immune response[1] permits antibodies to be generated against virtually any substance, catalytic antibodies have the potential to provide catalysts for many chemical transformations.[2-4] Such catalysts could be tailored by immunization with rationally designed transition state analogs, which is the main attraction of the catalytic antibody research field.[2,5-7] However, when mice are immunized with a hapten conjugated to a carrier protein, a few, and occasionally several, of the dozens of antibodies that bind the hapten are characterized as catalytic. The diversity of the immune response can provide a panel of catalytic antibodies that possess varying degrees of catalytic activity and substrate specificity.[8-12] These results have raised fundamental questions, such as the following: how do catalytic antibodies generated by immunization by a single hapten differ on a structural or mechanistic basis? Therefore, a central question in catalytic antibody research concerns the extent to which the rationally designed hapten dictates the paratopes for catalytic function in the antigen-

* To whom correspondence should be addressed.

[⊗] Abstract published in *Advance ACS Abstracts,* May 1, 1995.

(1) Davis, M. M.; Bjorkman, P. J. *Nature* **1988**, *334*, 395.
(2) Lerner, R. A.; Benkovic, S. J.; Schultz, P. G. *Science* **1991**, *252*, 659.
(3) Schultz, P. G.; Lerner, R. A. *Acc. Chem. Res.* **1993**, *26*, 391.
(4) Hilvert, D. *Acc. Chem. Res.* **1993**, *26*, 552.
(5) Jencks, W. *Catalysis in Chemistry and Enzymology;* McGraw-Hill: New York, 1969; p 228.
(6) Tramontano, A.; Janda, K. D.; Lerner, R. A. *Science* **1986**, *234*, 1566.
(7) Pollack, S. J.; Jacob, J. W.; Schultz, P. G. *Science* **1986**, *234*, 1570.
(8) Janda, K. D.; Weinhouse, M. I.; Danon, T.; Pacelli, K. A.; Schloeder, D. M. *J. Am. Chem. Soc.* **1991**, *113*, 5427.
(9) Angeles, T. S.; Smith, R. G.; Darsley, M. J.; Sugasawara, R.; Sanchez, R. I.; Kenten, J.; Schultz, P. G.; Martin, M. T. *Biochemistry* **1993**, *32*, 12128.
(10) Zemel, R.; Schindler, D. G.; Tawfik, D. S.; Eshhar, Z.; Green, B. S. *Mol. Immunol.* **1994**, *31*, 127.
(11) Suga, H.; Ersoy, O.; Tsumuraya, T.; Lee, J.; Sinskey, A. J.; Masamune, S. *J. Am. Chem. Soc.* **1994**, *116*, 487.
(12) Tarasow, T. M.; Lewis, C.; Hilvert, D. *J. Am. Chem. Soc.* **1994**, *116*, 7959.

0002-7863/95/1517-6199$09.00/0 

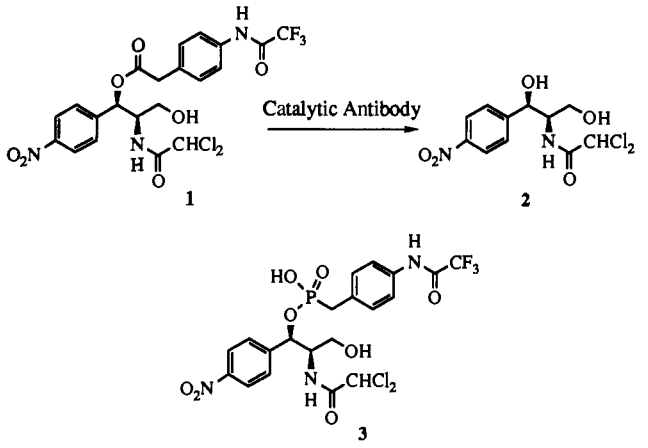


Figure 1.

combining site. We want to study the correlation between the antigen-combining-site structures and the chemical properties within a panel of catalytic antibodies elicited against a single hapten, which can potentially provide a more global understanding of the molecular mechanisms by which catalytic antibodies are generated in immune responses.

Previously, we have reported prodrug activation via catalytic antibodies that catalyze the hydrolysis of the nonbioactive chloramphenicol monoester derivative **1** to generate chloramphenicol **2**, as shown in Figure 1.[13] Immunization with a KLH conjugate of the transition state analog **3**, designed on the basis of the transition state stabilization concept, yielded 12 immunoglobulin G (Ig G) proteins binding to the hapten **3**, six of which were found to catalyze the hydrolysis with varying degrees of activity. This antibody system seems to be a suitable model for studies of the diversity of catalytic antibodies. We recently described the primary structures of the heavy and light chain variable regions of these 11 antibodies (including six catalytic and five noncatalytic antibodies) elicited against the haptenic phosphonate **3**.[14] Amino acid sequence cluster analysis, based on phylogenic trees constructed by the neighbor-joining method,[15] has revealed that the sequences of the noncatalytic antibodies bear no relationship to one another, while the catalytic antibodies share significant structural identity. The noncatalytic antibodies, 1G6, 3A7, 6A6, 7A11, and 9B7, have completely different sequences and show approximately 50% and 45% homology in the $V_L$ and $V_H$ regions, respectively. In accordance with the diversity of their primary structures, noncatalytic antibodies may have heterogeneous molecular interactions in the combining sites with the epitopes. On the other hand, the catalytic antibodies, 6D9, 8D11, 4B5, 9C10, and 3G6, share significant structural identity to one another and have 89−95% and 74−84% sequence homology in the complete $V_L$ and $V_H$ regions, respectively. The similarity of the primary structures suggests that these antibodies could belong to a shared idiotype family, in terms of the combining-site structure and the binding properties. The various degrees of catalytic activity observed in the hydrolysis of chloramphenicol monoester **1** seem to be due to limited differences in the amino acids in both the $V_L$ and $V_H$ chains.

Despite the antibody diversity, the fact that the group of catalytic antibodies has highly homogeneous variable region sequences within the anti-**3** antibodies suggests a limited number of modes of molecular interaction (antigen binding specificity)

(13) Miyashita, H.; Karaki, Y.; Kikuchi, M.; Fujii, I. *Proc. Natl. Acad. Sci. U.S.A.* **1993**, *90*, 5337.

(14) Miyashita, H.; Hara, T.; Tanimura, R.; Tanaka, F.; Kikuchi, M.; Fujii, I. *Proc. Natl. Acad. Sci. U.S.A.* **1994**, *91*, 6045.

(15) Saitou, N.; Nei, M. *Mol. Biol. Evol.* **1987**, *4*, 406.

**Table 1.** Kinetic Parameters of the Anti-**3** Antibody-Catalyzed Hydrolysis of Substrate **5**[a]

| antibody | $k_{cat}$ ($min^{-1}$) | $K_m$ ($\mu$M) | $k_{cat}/k_{uncat}$ | $K_S/K_{TSA}$[b] | $K_i$[c] ($\mu$M) | $K_m/K_i$ |
|---|---|---|---|---|---|---|
| 6D9 | 0.145 | 50 | 895 | 900 | 0.06[d] | 833 |
| 7C8 | 0.115 | 3.8 | 707 | 12 | 0.31 | 12 |
| 8D11 | 0.037 | 14.2 | 254 | 342 | | |
| 4B5 | 0.046 | 5.8 | 281 | 381 | | |
| 9C10 | 0.008 | 2.5 | 56 | 60 | | |
| 3G6 | 0.010 | 59.5 | 66 | 20 | | |

[a] Reaction conditions: 25 °C, 10% DMSO/50 mM Tris, pH 8.0. The first-order rate constant of the hydrolysis reaction without antibody ($k_{uncat}$) was $1.62 \times 10^{-4}$ $min^{-1}$. [b] $K_S$ and $K_{TSA}$ were determined by CIEIA, using substrate **5** and transition state analog **3**, respectively, as inhibitors. See the Experimental Section. [c] Against transition state analog **3**. [d] $K_i$ value was taken from ref 13.

**Scheme 1**

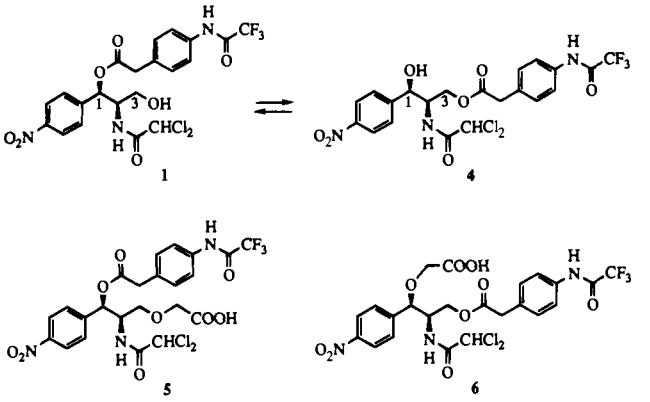


of the paratopes with epitopes for inducing catalytic activity in the antigen-combining sites. An exception is antibody 7C8, which was found to be catalytic, but its structure was different from the other catalytic antibodies, with 55% and 44% amino acid sequence homology to the prototype 6D9 in $V_L$ and $V_H$, respectively. This analysis suggests that 7C8 binds to the substrate or hapten in a mode of molecular interaction different from that of the other antibodies. In this work, we report the detailed biochemical properties of the six anti-**3** catalytic antibodies, to enhance our understanding of the active site structure and function relationship assignments. Because the antibodies appear to hydrolyze chloramphenicol monoester **1** with varying efficiencies, but differ little in structure, it seemed possible that information regarding the structure−function relationships could be obtained by a simple inspection of the sequences.

## Results

**Catalytic and Binding Assays.** To survey the catalytic activity within the six catalytic antibodies (6D9, 7C8, 8D11, 4B5, 9C10, and 3G6) elicited with transition state analog **3**, the kinetic parameters of the antibody-catalyzed hydrolysis were determined (Table 1). Since the monoester of chloramphenicol **1** exists as an equilibrium mixture (**1** and **4**) of regioisomers at C-1 and C-3, the antibody-catalyzed hydrolysis proceeds along with isomerization of the ester group between C-1 and C-3 (Scheme 1). To exclude the kinetic complexity caused by the isomerization, substrate **5**, which is a derivative with an ether at the C-3 position in **1**, was prepared and used for the kinetic assays. The subtle structural change also improved the solubility of the substrate for the kinetic assays, due to the carboxylic acid of substrate **5**. When the antibody-catalyzed reactions with substrate **5** and the regioisomer **6** were examined, all six antibodies catalyzed hydrolysis with substrate **5**, but none

hydrolyzed the regioisomer **6**, confirming the strict regioselectivity programmed with the corresponding hapten **3**.

The antibody-catalyzed reactions were performed at 25 °C in 10% DMSO/50 mM Tris (pH 8.0) and were followed by HPLC detection of the alcohol product. All of the antibody-catalyzed hydrolyses proceeded according to Michaelis–Menten kinetics and were completely inhibited by the addition of the transition state analog **3**, used for the immunization, to the reaction mixture. The first-order rate constants per antigen-combining site ($k_{cat}$) and Michaelis constants ($K_m$) in the six catalytic antibodies were in the range of 0.008–0.145 $min^{-1}$ and 2.5–60 $\mu$M, respectively, as shown in Table 1. Dixon analyses of antibodies 6D9 and 7C8 with **3** afforded inhibition constants ($K_i$) of 0.06 and 0.31 $\mu$M, respectively. The hydrolysis with antibody 6D9 (5 $\mu$M) proceeded with complete consumption of substrate **5** (200 $\mu$M) in 180 min, without detectable product inhibition.

According to transition state theory,[16] under ideal conditions, one can predict the rate enhancement of an antibody-catalyzed reaction from the ratio of the affinity for the substrate relative to the affinity for the transition state. If a hapten is a true analog of the actual transition state of the reaction and does not contain extraneous structural features that are not present in its corresponding substrate, the ratio of the dissociation constants for the transition state analog ($K_{TSA}$) and the corresponding substrate ($K_S$) should then be equal to the rate enhancement ($k_{cat}/k_{uncat} = K_S/K_{TSA}$).[17-20] A number of antibodies specific for phosphonate transition state analogs has shown close agreement between experimentally derived $k_{cat}/k_{uncat}$ and $K_S/K_{TSA}$ ratios.[9,17] This concept also has been exploited for many years to provide evidence that an inhibitor is a transition state analog of an enzyme-catalyzed reaction.[21-27] Since we have generated monoclonal antibodies against the putative transition state analog, with the expectation that the antibodies may be catalytic by virtue of the theoretical relationship between the affinity for the transition state and the catalytic efficiency, the ratio of the affinity ($K_S$) for substrate **5** relative to the affinity ($K_{TSA}$) for the transition state analog **3** within the six catalytic antibodies was determined by competitive inhibition enzyme immunoassay (CIEIA)[28,29] and was analyzed on the basis of transition state theory.

Figure 2 shows plots of $k_{cat}/k_{uncat}$ versus $K_S/K_{TSA}$ for the six catalytic antibodies. Although the catalytic antibodies possess varying values of $K_m$, $k_{cat}$, $K_S$, and $K_{TSA}$, the transition state analysis displays a linear relationship among antibodies 6D9, 8D11, 4G5, and 9C10. The slope of the straight line is 0.99. This suggests that the entire differential binding energy of the four catalytic antibodies to the transition state vs the ground state might be available for rate enhancement. On the other hand, the plots for antibodies 7C8 and 3G6 deviate from the linear relationship, suggesting that factors other than transition state stabilization, such as a functioning acid or base or nucleophilic catalyst, are involved in the catalysis.

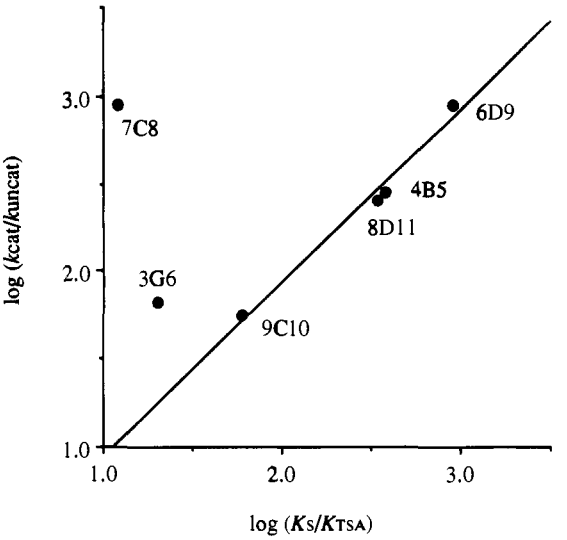


**Figure 2.** Plot of $\log(K_S/K_{TSA})$ versus $\log(k_{cat}/k_{uncat})$ for catalytic antibodies generated against phosphonate transition state analog **3**. A linear relationship was obtained for antibodies 6D9, 4B5, 8D11, and 9C10, suggesting that the antibody-combining sites act as catalysts by stabilizing the transition state; slope = 0.99, $R^2 = 0.98$. Data represented in this figure are in Table 1.

**Substrate Specificities.** The catalytic antibodies 6D9, 9C10, 8D11, 3G6, 4G5, and 7C8 were selected for binding activity to the transition state analog **3** and for hydrolytic activity against monoester **1**, but not for the presence of a related structure in the region of the antigen-combining site (*i.e.*, a related idiotype). However, the catalytic antibodies 6D9, 8D11, 4B5, 9C10, and 3G6 (except 7C8) shared significant amino acid sequence identity to one another in the complete $V_L$ and $V_H$ regions, suggesting closely related structures in the region of the antigen-combining site within these antibodies. Therefore, to confirm that the catalytic antibodies belong to a shared idiotype family in terms of combining-site structures and binding properties, the substrate specificity of the antibodies was examined using substrate **5** and its derivative **7**, in which the trifluoroacetyl group

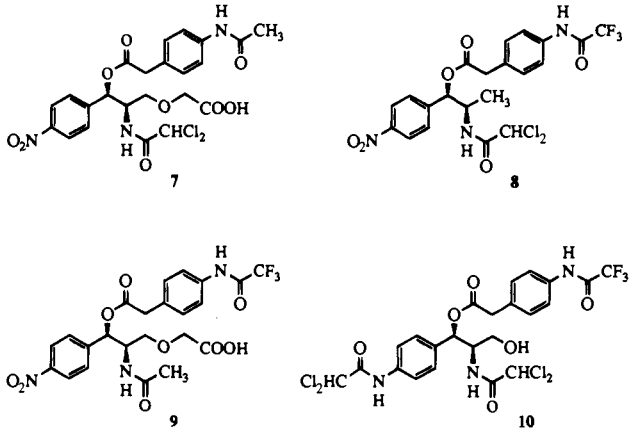


of **5** was converted to an acetyl group.[6,30,31] If the combining-site structures and the binding modes to the hapten and the substrates of these catalytic antibodies are related each other, the antibodies should display a homologous substrate specificity.

(16) Eyring, H. *J. Chem. Phys.* **1935**, *3*, 107.
(17) Jacobs, J. W. *Bio/Technology* **1991**, *9*, 258.
(18) Leinhard, G. E. *Science* **1973**, *180*, 149.
(19) Wolfenden, R.; Frick, L. *Enzyme Mechanisms*; Page, M. I., Williams, A., Eds.; Royal Society of Chemistry: London, 1987.
(20) Kraut, J. *Science* **1988**, *180*, 149.
(21) Brady, K.; Abeles, R. H. *Biochemistry* **1990**, *29*, 7608.
(22) Westerlik, J. O.; Wolfenden, R. *J. Biol. Chem.* **1972**, *247*, 8195.
(23) Thompson, R. C. *Biochemistry* **1973**, *12*, 47.
(24) Thompson, R. C.; Bauer, C. A. *Biochemistry* **1979**, *18*, 1552.
(25) Bartlett, P. A.; Marlowe, C. K. *Biochemistry* **1983**, *22*, 4618.
(26) Hanson, J. E.; Kaplan, A. P.; Bartlett, P. A. *Biochemistry* **1989**, *28*, 6294.
(27) Nair, H. K.; Seravalli, J.; Arbuckle, T.; Quinn, D. M. *Biochemistry* **1994**, *33*, 8566.
(28) Rath, S.; Stanley, C. M.; Steward, M. W. *J. Immunol. Methods* **1988**, *106*, 245.
(29) This method probably underestimates the true binding constants ($K_S$ and $K_{TSA}$) but is useful in determining the ratio of $K_S$ relative to $K_{TSA}$.
(30) Tramontano, A.; Janda, K. D.; Lerner, R. *Proc. Natl. Acad. Sci. U.S.A.* **1986**, *83*, 6736.
(31) Tramontano, A.; Ammann, A. A.; Lerner, R. *J. Am. Chem. Soc.* **1988**, *110*, 2282.

**Table 2.** Relative Efficiencies of Anti-**3** Catalytic Antibodies for Hydrolysis of Substrates **5** and **7**[a]

| antibody | relative velocities[b] | |
|---|---|---|
| | substrate **5** | substrate **7** |
| 6D9 | 100 | 7 |
| 7C8 | 105 | 91 |
| 8D11 | 61 | 10 |
| 4B5 | 47 | 7 |
| 9C10 | 25 | 2 |
| 3G6 | 14 | 4 |

[a] Reaction conditions: 5 $\mu$M of antibody and 200 $\mu$M of substrate in 10% DMSO/50 mM Tris, pH 8.0, at 25 °C. [b] Relative velocities were determined by comparing the hydrolysis of substrate **5** with antibody 6D9.

**Table 3.** Kinetic Parameters of the Hydrolysis by Antibodies 6D9 and 7C8[a]

| antibody | | substrate | | |
|---|---|---|---|---|
| | | **7** | **8** | **9** |
| 6D9 | $k_{cat}$ (min$^{-1}$) | 0.030 | 0.033 | 0.012 |
| | $K_m$ ($\mu$M) | 515 | 56 | 255 |
| | $k_{cat}/k_{uncat}$[b] | 204 | 934 | 155 |
| 7C8 | $k_{cat}$ (min$^{-1}$) | 0.123 | 0.070 | 0.007 |
| | $K_m$ ($\mu$M) | 12 | 6.0 | 4.2 |
| | $k_{cat}/k_{uncat}$[b] | 840 | 1989 | 97 |

[a] Reaction conditions: 25 °C, 10% DMSO/50 mM Tris, pH 8.0. [b] The first-order rate constants of the hydrolyses of substrates **7**, **8**, and **9** without antibody ($k_{uncat}$) were $1.5 \times 10^{-4}$, $3.5 \times 10^{-5}$, and $7.5 \times 10^{-5}$ min$^{-1}$, respectively.

Table 2 shows the relative velocities for substrates **5** and **7** in the antibody-catalyzed hydrolysis with the six catalytic antibodies, under the conditions of 5 $\mu$M antibody and 200 $\mu$M substrate in 10% DMSO/50 mM Tris (pH 8.0). Although antibodies 6D9, 8D11, 4B5, 9C10, and 3G6, with highly homologous amino acid sequences, hydrolyzed substrate **5** with varying degrees of catalytic activity, all five antibodies displayed reduced catalytic activities for **7**, with rates of 3.5−14 times lower than those for **5**. On the other hand, antibody 7C8, with an amino acid sequence different from those of the other five antibodies, was found to catalyze the hydrolysis of substrate **5** and **7** with the same rate enhancement. Thus, antibody 7C8 displayed substrate specificity different from those of the other catalytic antibodies, which is consistent with the difference in the amino acid sequences of the Fv regions.

In addition, we have examined the substrate specificity of prototypes 6D9 and 7C8 in detail, using other substrates, **8**, **9**, and **10**. The kinetic parameters in the antibody-catalyzed hydrolyses of substrates **7**, **8**, and **9** are shown in Table 3. Neither 6D9 nor 7C8 displayed catalytic activity for **10**, which bears a bulky *p*-dichloroacetamido group instead of the *p*-nitro group. Substrate **8** was found to be a good substrate for both 6D9 and 7C8, with a $K_m$ value and a rate enhancement ($k_{cat}/k_{uncat}$) comparable to those of **5**. Any structural change at the C-3 position should not affect the antibody−substrate interaction because the hapten was conjugated with a bulky carrier protein at the C-3 position. Both antibodies 6D9 and 7C8 had reduced hydrolytic activities with substrate **9**, which has an acetylamide derivative at the C-2 position. As noted above, a dramatic difference in the substrate specificity between antibodies 6D9 and 7C8 was observed in the hydrolysis of substrate **7**. This suggests that the *p*-((*N*-trifluoroacetyl)amino)phenyl group in the hapten is one of the essential epitopes for 6D9, but not for 7C8.

**Chemical Modifications.** Chemical modification of the antibodies showed that the hydrolytic activity for substrate **5** was reduced by arginine-, tyrosine-, and especially histidine-specific reagents. Upon treatment of the antibodies with phenylglyoxal[32] at a 150:1 molar ratio of reagent/protein to modify the arginine residues, all six antibodies lost 50−70% of the activity. Nitration of tyrosine residues by tetranitromethane[33] at a 100:1 molar ratio of reagent/protein reduced the activity of the antibodies by 60−75%, with the exception of antibody 3G6. The partial loss of activity can be interpreted as being due to a conformational change in the protein following reaction of the reagents at amino acid residues somewhere other than in the binding site. In the case of antibody 3G6, treatment with tetranitromethane completely abolished the hydrolytic activity, suggesting that a tyrosine residue critical for the hydrolytic activity or binding affinity exists in the binding site.

A dramatic difference within the set of catalytic antibodies was observed in the chemical modification with diethyl pyrocarbonate[34] (DEPC). When all six catalytic antibodies were treated with DEPC, in a 25-fold molar excess to the active site in neutral buffer (50 mM sodium phosphate, pH 7.0) to modify any histidine residues, antibodies 6D9, 8D11, 4B5, and 9C10 completely lost the hydrolytic activity. The profound effect of the modification with DEPC suggests that an imidazole group is participating in the hydrolytic reactions of antibodies 6D9, 8D11, 4B5, and 9C10. Antibody 3G6 had a 40% reduction in activity under the same conditions. On the other hand, antibody 7C8 resisted chemical modification with DEPC under the same conditions and retained the same activity as that before the modification.

Although DEPC can react with the functional groups of a variety of amino acid residues, the usual group modified in neutral or slightly acidic media is the histidine imidazole. To provide further evidence for an essential histidine in the antibodies, we have examined the reactivation of the DEPC-modified antibody 6D9 with hydroxylamine.[34] Treatment of the modified antibody 6D9 (with <2% original activity) with 25 mM hydroxylamine for 15 min reversed the inactivation by >85%. In general, reaction of DEPC with lysine or arginine is irreversible, and tyrosine modification is considerably slower in its reversal. Although the possibility cannot be ruled out that modification of a histidine distal to the active site causes an inactive enzyme conformation, the results are clearly consistent with an essential active site histidine in antibody 6D9.

**pH Profiles.** As discussed above, the ratio of $k_{cat}/k_{uncat}$ shows a linear relationship with the ratio of $K_S/K_{TSA}$ in the antibody-catalyzed reactions with 6D9, 8D11, 4B5, and 9C10, proving that the hapten is an ideal transition state mimic and that the binding interaction directed to the phosphonate moiety of the hapten only helps to stabilize a transition state or tetrahedral intermediate of this reaction. On the other hand, antibody 7C8 displayed a rate enhancement too large to be rationalized solely by transition state binding energy. These results led us to postulate that chemical catalysis (*e.g.*, general acid−general base and/or nucleophilic) may be involved in the antibody-catalyzed reaction with antibody 7C8, but not with antibody 6D9, which might be detected in pH profile studies.

The pH dependence of antibodies 6D9 and 7C8 in the hydrolysis of substrate **5** was examined between pH 6.0 and 8.5 (Figure 3). Reactions above pH 8.5 could not be followed, due to the rapid spontaneous degradation of substrate **5**. The catalytic activity of antibody 6D9 shows a linear dependence on hydroxide ion concentration in the pH range. It thus appears that hydroxide ions directly attack the antibody-bound substrate and that the resulting transition state is stabilized in the antigen-

(32) Takahashi, K. *J. Biol. Chem.* **1968**, *243*, 6171.
(33) Cuatrecasas, P.; Fuchs, S.; Anfinsen, C. B. *J. Biol. Chem.* **1968**, *243*, 4787.
(34) Miles, E. W. *Methods Enzymol.* **1977**, *47*, 431.

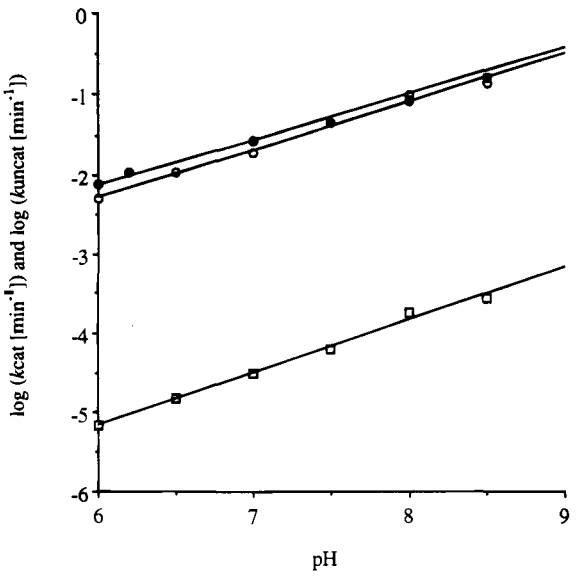


**Figure 3.** pH profiles of log $k_{cat}$ for the antibody 6D9 (○) and antibody 7C8 (●) catalyzed hydrolysis of substrate **5** and log $k_{uncat}$ (□) for the background hydrolysis of substrate **5**.

combining site. In the antibody-catalyzed reaction with antibody 7C8, we also observed a linear pH dependence of $k_{cat}$. While this appears to contradict our prediction described above, there exists the possibility that the p$K_a$'s of the catalytic residues may lie outside the pH range investigated.

**Three-Dimensional Structure Model.**[35] In the absence of high-resolution structural data for antibody 6D9, a three-dimensional computer model of the antigen-combining site was constructed in order to understand the observed biochemical properties. To start the model building of antibody 6D9, the crystal structure of the antibody B13I2 Fab fragment complexed with the peptidic hapten (Protein Data Bank[36] [PDB] code 2IGF)[37] was chosen as a template for the following reasons: (i) the amino acid sequences of the heavy and light chains in the variable regions of B13I2 are 73% and 91% identical to those of antibody 6D9, respectively, (ii) each CDR loop of L1, L2, L3, and H1 in antibodies 6D9 and B13I2 belongs to the identical canonical structural class.

The uncomplexed model of antibody 6D9 displays a concave, bowl-like shape of the antigen-combining site, which is quite similar to that of antibody B13I2. The crystal structure of antibody B13I2 reveals a cavity formed by Phe (H100k), Phe (L89), Trp (H47), Pro (L96), and Tyr (H95) at the center of the antigen-combining site, in which a histidine residue in the peptidic antigen is bound. Such a cavity is also observed in the model of antibody 6D9 and is formed by Phe (H100k), Phe (L89), Trp (H47), Pro (L96), and Val (H95). Replacement of the bulky tyrosine residue with valine at the position of H95 makes the cavity in antibody 6D9 deeper and more hydrophobic than that in antibody B13I2. As a next step in the model building, we docked the transition state analog **3** into the antigen-combining site, based on the information obtained from the study of the substrate specificity for antibody 6D9. The phosphonate transition state analog **3** possesses two hydrophobic functional groups, *p*-((*N*-trifluoroacetyl)amino)phenyl and *p*-nitrophenyl groups, which were expected to fill the hydrophobic pocket. The substrate specificity suggests that the trifluoroacetyl group in the transition state analog **3** is one of the essential epitopes for antibody 6D9 and that the position C-3, at which the transition state analog **3** was conjugated with the bulky carrier protein, is outside the antigen-combining site. Consequently, the *p*-((*N*-trifluoroacetyl)amino)phenyl group is placed in the hydrophobic pocket and the *p*-nitrophenyl group was laid on the groove formed by the H1 and H3 loops (Figure 4).

The location of the transition state analog **3** immediately demonstrated that the imidazole group of the L1 loop His (L27d), positioned at the edge of the antigen-combining site, binds to the phosphorus oxyanion of the hapten by hydrogen bonding or an electrostatic interaction. This model is supported by examination of the crystallographic structures of the antibodies TE33 (PDB code 1TET),[38] DB3 (PDB code 1DBJ),[39] Bv04−01 (PDB code 1CBV),[40] and 4−4−20 (PDB code 4FAB),[41] which possess homologous amino acid sequences and the identical L1 canonical class as antibody 6D9: it is observed that the imidazole side chain of His at the same position (L27d) is directed into the antigen-combining site and participates in the antigen binding. Thus, the model of the antibody 6D9−antigen complex strongly suggests that the His at the position of L27d is the amino acid residue functioning in the antibody-catalyzed hydrolysis.

## Discussion

A central question in catalytic antibody development concerns the extent to which the rationally designed hapten dictates the paratopes for catalytic function in the antigen-combining site. In this work, therefore, we have investigated the biochemical properties within a panel of catalytic antibodies elicited against a single transition state analog and have examined the correlation between the functions and the antigen-combining-site structures.

Because the catalytic antibodies discussed here were generated against the putative transition state analog, with the expectation that the antibodies may be catalytic by virtue of the theoretical relationship between the affinity of the transition state and the catalytic efficiency, we have studied the effect of antibody−hapten complementarity on the catalytic properties by comparing the kinetic properties within the antibodies. In plots of $k_{cat}/k_{uncat}$ versus $K_S/K_{TSA}$ for the six catalytic antibodies (Figure 2), a linear relationship was observed for the hydrolysis with the four antibodies 6D9, 8D11, 4D5, and 9C10, with highly homologous primary amino acid sequences, providing evidence that some interactions used by the antibodies in hapten binding are also used in transition state binding to accelerate the hydrolysis. Thus, these four antibodies catalyze the hydrolysis of substrate **5** by variations of the same basic mechanism of transition state stabilization. In addition, the magnitude (0.99) of the slope ($R^2$ = 0.98) in Figure 2 suggests that the entire differential binding energy to the transition state vs the ground state is available for the rate enhancement.[9,17,21,25,26] Consequently, the transition state analog **3** used for the immunization might be a "perfect" hapten that exactly matches the transition state structure of the uncatalyzed reaction and does not contain extraneous structural features that are not present in its corresponding substrate. Since any changes in antibody structure would have the same effect on the hapten binding energy as on

(35) The amino acid residues in the model are numbered according to Kabat *et al.*: Kabat, E. A.; Wu, T. T.; Perry, H. M.; Gottesman, K. S.; Foeller, C. *Sequences of Proteins of Immunological Interest*, 5th ed.; U.S. Public Health Service, National Institute of Health: Bethesda, MD, 1991.

(36) Bernstein, F. C.; Koetzle, T. F.; Williams, G. J. B.; Meyer, E. F., Jr.; Rogers, J. R.; Kennard, O.; Shimanouchi, T.; Tasumi, M. *J. Mol. Biol.* **1977**, *112*, 535.

(37) Stanfield, R. L.; Fieser, T. M.; Lerner, R. A.; Wilson, I. A. *Science* **1990**, *248*, 712.

(38) Shoham, M. *J. Mol. Biol.* **1993**, *232*, 1169.

(39) Arevalo, J. H.; Taussig, M. J.; Wilson, I. A. *Nature* **1993**, *365*, 859.

(40) Herron, J. N.; He, X. M.; Ballard, D. W.; Blier, P. R.; Pace, P. E.; Bothwell, A. L. M.; Voss Junior, E. W.; Edmundson, A. B. *Proteins: Struct., Funct., Genet.* **1991**, *11*, 159.

(41) Herron, J. N.; He, X.; Mason, M. L.; Voss Junior, E. W.; Edmundson, A. B. *Proteins: Struct., Funct., Genet.* **1989**, *5*, 271.

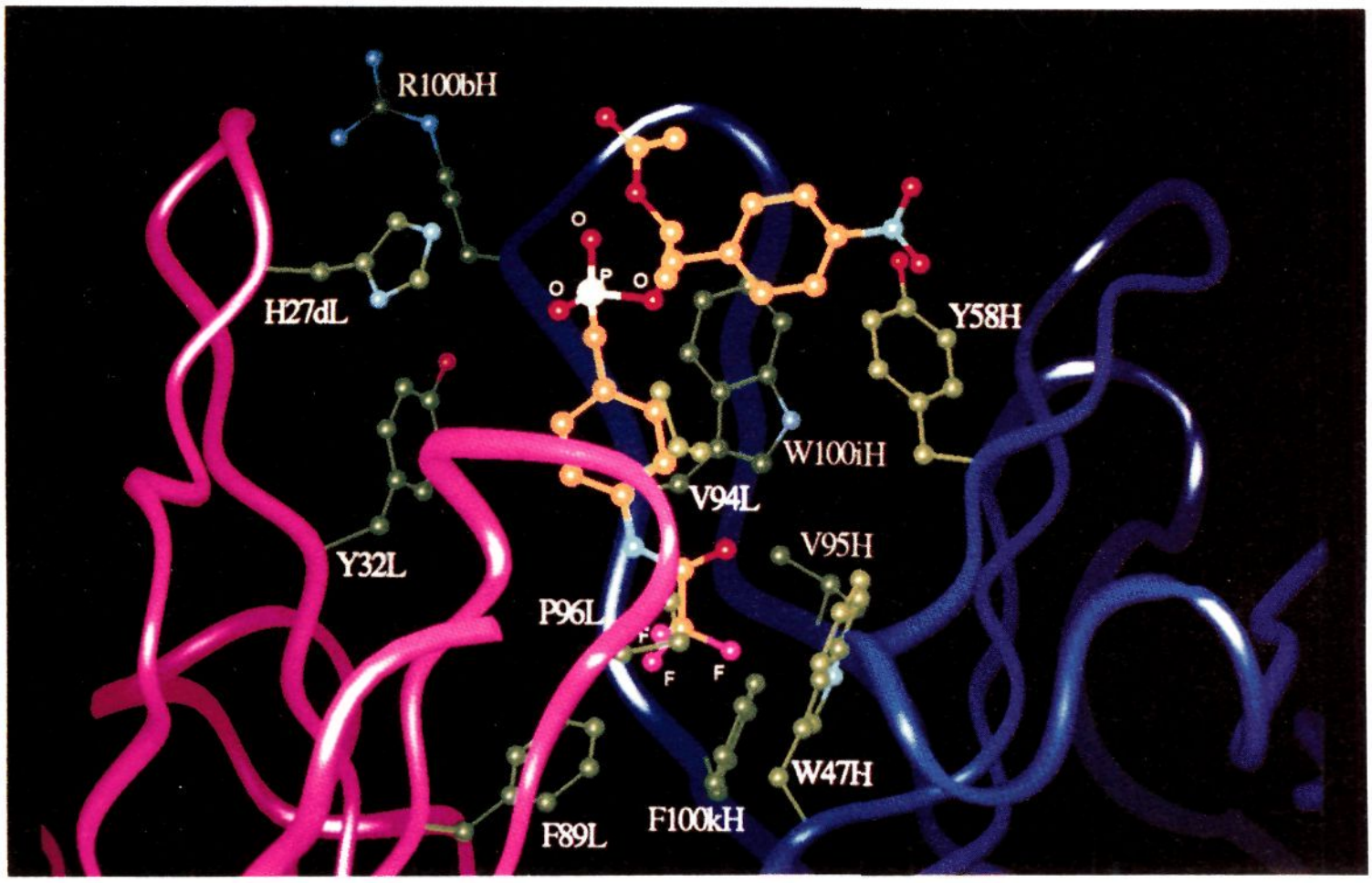


**Figure 4.** Three-dimensional model of the complex of antibody 6D9 (Fv) with transition state analog **3**. The light and heavy chains are shown with purple ribbon on the left and blue ribbon on the right, respectively. The amino acid residues are represented by one letter amino acid notion and are numbered according Kabat *et al.*[35] The carbon atoms of the side chains and the hapten are displayed in green and in yellow, respectively. The other atoms are colored as follows: N (cyan), O (red), P (white), and F (purple). The dichloroacetamido moiety of the hapten **3**, which locates in the front of the phosphonate moiety in the model, is not shown in this figure.

the transition state binding energy, it appears likely that the varying degrees of catalytic activity among these catalytic antibodies probably result from subtle structural changes in the antigen-combining sites.

In the prototype 6D9, the difference ($\Delta\Delta G$) in free energy between the antibody-catalyzed and uncatalyzed (background) reactions and the difference ($\Delta\Delta G$) in the binding energy between the transition state and the ground state were calculated, based on the values of $k_{cat}/k_{uncat}$ and $K_S/K_{TSA}$, respectively, to be 4.0 kcal/mol for both.[42] This value is consistent with the typical binding energy for one hydrogen bond between charged and uncharged groups in enzyme−substrate (or inhibitor) complexes (~4 kcal/mol).[43,44] On the other hand, the plots for antibodies 7C8 and 3G6 in Figure 2 deviate from the linear relationship. The calculated differential free energies (3.9 kcal/mol for antibody 7C8 and 2.5 kcal/mol for antibody 3G6) for the rate enhancements are not consistent with the differential binding energies (1.5 kcal/mol for antibody 7C8 and 1.8 kcal/mol for antibody 3G6) between the transition state and the ground state.[42] This suggests that catalytic factors other than transition state stabilization, such as a functioning acid or base or nucleophilic catalyst, are involved in the catalysis with antibodies 7C8 and 3G6. The transition state analysis discussed above demonstrates the difference in the catalytic properties between the antibodies 7C8 and 3G6 and the other four antibodies, which is reflected in the differences in the Fv amino acid sequences. Although antibody 3G6 has high sequence homology to the other four catalytic antibodies, antibody 3G6 has Tyr (L27d) instead of His (L27d), which is the functional amino acid residue in the four antibodies with highly homogeneous amino acid sequences (*vide infra*).

Because the primary amino acid sequences of the catalytic antibodies 6D9, 8D11, 4B5, 9C10, and 3G6 were found to be homogeneous,[14] it would be expected that valuable information about the functional amino acid residues can be obtained by comparing their sequences. However, even though the antibodies possess homogenous amino acid sequences, they do not always interact with the antigen in the same binding mode. Therefore, it is necessary for the sequence comparison to confirm that the catalytic antibodies belong to a shared idiotype family, in terms of combining site structures and binding properties. The analysis of the substrate specificity within the set of catalytic antibodies suggests that antibodies 6D9, 8D11, 4B5, 9C10, and 3G6 possess homogeneous binding modes for the substrate or hapten, while antibody 7C8 binds in a mode of molecular interaction different from that of the other antibodies. This is also reflected in the difference in the amino acid sequences in the Fv regions. The observed homogeneous substrate specificity within these five antibodies, 6D9, 8D11, 4B5, 9C10, and 3G6, could permit further analysis of their amino acid sequences to determine which structural differences in the antigen-combining sites could be correlated with catalytic activity.

The three-dimensional molecular model of the antibody 6D9−hapten complex was constructed on the basis of the amino acid sequence in the Fv region and the antigen-binding mode inferred by examination of the substrate specificity (Figure 4). The model indicates some structural characteristics of the antibody−hapten complex and shows that the phosphonate moiety in the hapten interacts with His (L27d) in CDR 1 of the light chain and that the *p*-((*N*-trifluoroacetyl)amino)phenyl group is in the hydrophobic pocket formed by Phe (H100k), Phe (L89), Trp (H47), Pro (L96), and Val (H95). Considering this model, we

(42) These energies were calculated from $\Delta\Delta G = RT \ln(k_{cat}/k_{uncat})$ and $\Delta\Delta G = RT \ln(K_S/K_{TSA})$.

(43) Fersht, A. R.; Shi, J.-P.; Knill-Jones, J.; Lowe, D. M.; Wilkinson, A. J.; Blow, D. M.; Brick, P.; Carter, P.; Waye, M. M. Y.; Winter, G. *Nature* **1985**, *314*, 235.

(44) Bartlett, P. A.; Marlowe, C. K. *Science* **1987**, *235*, 569.

examined the amino acid sequences of the Fv regions within the five antibodies 6D9, 8D11, 4B5, 9C10, and 3G6. We found that the His (L27d) in the CDR 1 of the light chain is conserved in the catalytic antibodies 6D9, 8D11, 4B5, 9C10, while antibody 3G6 has a tyrosine residue at the corresponding position. We suspected, therefore, that the His at position L27d is a catalytic amino acid residue participating in transition state stabilization in the antibody-catalyzed reactions. Our proposal regarding the catalytic amino acid residues is conformed by the susceptibility of these catalytic antibodies to a variety of chemical modifications. Treatment of antibodies 6D9, 8D11, 4B5, and 9C10 with DEPC, to modify essential histidine residues, destroyed the hydrolytic activity. While antibody 3G6 partially lost activity with the histidine modification, treatment with tetranitromethane completely abolished the activity, suggesting that tyrosine is a crucial amino acid residue for the hydrolytic activity.

Together with the transition state analysis discussed above, the indication that a histidine is critical to the hydrolytic activities of antibodies 6D9, 8D11, 4B5, and 9C10 provides a scenario regarding reaction mechanisms. A possible reaction mechanism of the antibody-catalyzed reactions is that a histidine acts to stabilize the transition state in a manner similar to that for the histidine in thermolysin, as reported by Monzingo and Matthew.[45] Thus, the histidine (L27d) in the antigen-combining site might be involved in the stabilization of the transition state by forming an hydrogen bond with the oxyanion of the hydrated ester. Although the role of the imidazole group of histidine as a nucleophilic and general base catalyst in ester hydrolysis is well established, the kinetic studies showing that antibody 6D9 turned over several hundred fold with substrate **5**, without either burst kinetic or noticeable reaction inhibition, and the pH profile of antibody 6D9, which shows a linear dependence on hydroxide ion concentration between pH 6.0 and 8.5, might rule out the possibility of the histidine functioning as a nucleophilic and general base catalyst.

In this study, we examined on the correlation between the structures and the functions within a set of catalytic antibodies generated against a single transition state analog. As a result, it has been shown that the differences in the biochemical properties within these antibodies are consistent with the differences in the amino acid sequences. It is noteworthy that the majority of these catalytic antibodies generated against a single transition state analog display high homology in the biochemical and structural propertie and catalyze the reaction with the same mechanism expected from designing the transition state analog. Although catalytic antibody technology is still dependent on the sophisticated biological immune system and screening procedures, this result emphasizes the critical importance of hapten affinity to transition state stabilization and of chemically designing haptens that closely resemble the true transition state for the generation of catalytic antibodies. Comparative studies of the structurally and mechanistically similar catalytic antibodies have greatly assisted in the elucidation of the reaction mechanism and the identifications of some obvious key amino acid residues. These data serve as an important introduction to the structural and mechanistic considerations that may be extended or modified by affinity labeling, site-directed mutagenesis, and structural determination studies. Such information will be helpful for the future design and generation of catalytic antibodies with improved activity.

## Experimental Section

**General Methods (Synthesis).** All oxygen or moisture sensitive reactions were carried out under argon. Flash chromatography was performed using Kisel gel (230–400 mesh) silica gel (Merck). Preparative thin-layer chromatography (TLC) was performed on Kisel gel 60 $F_{254}$ (0.5 mm) (Merck). Preparative high-performance liquid chromatograpy (HPLC) was performed on a Hitachi L-6200 equipped with a L-4200 UV detector. $^1$H NMR spectra were recorded on Bruker AM 500 (500 MHz) and AMX 600 (600 MHz) NMR spectrometers. The spectra are reported in units of ppm downfield from tetramethylsilane. Mass spectra were recorded with a JEOL JMS-SX102/102A (Tandem MS) mass spectrometer.

**Compound 11.** NaH (60% in oil, 106.0 mg, 2.65 mmol) was added

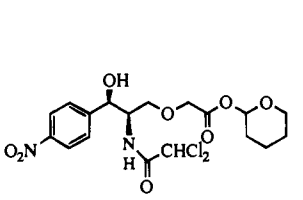

**11**

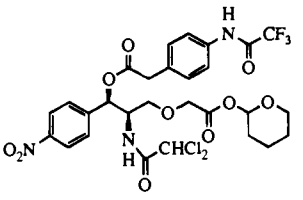

**12**

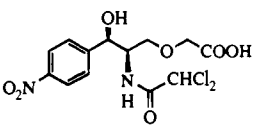

**13**

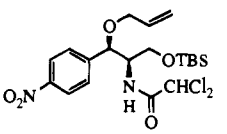

**14**

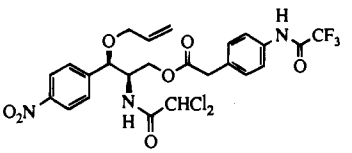

**15**

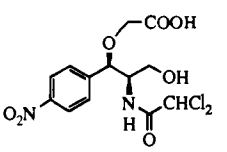

**16**

to a solution of chloramphenicol (650.3 mg, 2.01 mmol) in THF (7.0 mL) at 0 °C, and after 10 min, a solution of (tetrahydropyranyl)-iodoacetic acid (739 mg, 2.74 mmol) in THF (4.0 mL) was added. After the reaction mixture was stirred at 0 °C for 80 min, the reaction was quenched with saturated aqueous $NH_4Cl$ and the reaction mixture was extracted with EtOAc. The combined organic layers were washed with brine, dried over $MgSO_4$, filtered, concentrated *in vacuo*, and flash chromatographed (hexane/EtOAc = 1:1 and 1:2) to give **11** as a colorless gum (365.5 mg, 39%). The gum was crystallized from hexane–EtOAc to give **11** as colorless crystals. $^1$H NMR (500 MHz, $CDCl_3$–$CD_3OD$) (crystallized one isomer): $\delta$ 8.20 (m, $J_{ortho}$ = 8.7 Hz, 2H), 7.57 (m, $J_{ortho}$ = 8.7 Hz, 2H), 5.80 (s, 1H), 5.06 (m, 1H), 4.72 (m, 1H), 4.46 (dd, $J$ = 6.3 Hz, 10.4 Hz, 1H), 4.41 (m, 1H), 4.33 (dd, $J$ = 6.0 Hz, 10.4 Hz, 1H), 4.26 (AB, $J$ = 16.5 Hz, $\Delta\nu$ = 6.6 Hz, 2H), 3.86 (m, 1H), 3.35 (m, 1H), 1.90–1.52 (m, 6H). FDMS: *m/z* 465 ($M^+$).

**Compound 12.** A solution of **11** (80.0 mg, 0.172 mmol), 4-((trifluoroacetyl)amino)phenylacetic acid[46] (46.7 mg, 0.189 mmol), and 1-(3-(dimethylamino)propyl)-3-ethylcarbodiimide hydrochloride (EDC) (45.3 mg, 0.236 mmol) in pyridine (1.0 mL) was stirred at room temperature for 18 h. The solvent was removed *in vacuo*. The mixture was treated with saturated aqueous $NH_4Cl$ and was extracted with EtOAc. The combined organic layers were washed with brine, dried over $MgSO_4$, filtered, concentrated *in vacuo*, and flash chromatographed (hexane/EtOAc = 1:1) to give **12** as a colorless gum (53.1 mg, 44%). $^1$H NMR (500 MHz, $CDCl_3$) (mixture of two isomers): $\delta$ 8.18 (m, $J_{ortho}$ = 8.6 Hz, 2H), 8.09 (bs, 1H), 7.56 (m, $J_{ortho}$ = 8.6 Hz, 2H), 7.41 (m, $J_{ortho}$ = 8.6 Hz, 2H × 0.5), 7.40 (m, $J_{ortho}$ = 8.6 Hz, 2H × 0.5),

(45) Monzingo, A. F.; Matthew, B. W. *Biochemistry* **1984**, *23*, 5724.

(46) Janda, K. D.; Ashley, J. A.; Jones, T. M.; McLeod, D. A.; Schloeder, D. M.; Weinhouse, M. I.; Lerner, R. A.; Gibbs, R. A.; Benkovic, P. A.; Hilhorst, R.; Benkovic, S. J. *J. Am. Chem. Soc.* **1991**, *113*, 291.

7.30 (m, $J_{ortho}$ = 8.6 Hz, 2H), 6.68–6.65 (m, 1H), 6.05–6.02 (m, 1H), 4.71–4.68 (m, 1H), 4.62–4.56 (m, 1H), 4.22 (s, 2H), 4.22–4.15 (m, 1H), 4.08–4.01 (m, 1H), 3.87–3.81 (m, 1H), 3.74 (s, 2H), 3.55–3.50 (m, 1H), 1.88–1.48 (m, 6H). FABMS: *m/z* 694 ($M^+ + H$). HR-FABMS: calcd for $C_{28}H_{29}{}^{35}Cl_2F_3N_3O_{10}$ ($M^+ + H$) 694.1182, found 694.1181.

**Compound 5.** To a solution of **12** (171.2 mg, 0.247 mmol) in acetone (2.0 mL) was added 10% aqueous HCl (0.2 mL) at room temperature. After 30 min, the reaction mixture was diluted with water and the acetone was removed *in vacuo*. The mixture was extracted with EtOAc. The combined organic layers were washed with brine, dried over $MgSO_4$, filtered, concentrated *in vacuo*, and flash chromatographed (hexane/EtOAc = 1:2) to give **5** as a colorless gum (125.3 mg, 83%). The gum was crystallized from hexane–EtOAc to give **5** as colorless crystals. $^1$H NMR (500 MHz, $CDCl_3$–$CD_3OD$): $\delta$ 8.20 (m, $J_{ortho}$ = 8.7 Hz, 2H), 7.61 (m, $J_{ortho}$ = 8.7 Hz, 2H), 7.44 (m, $J_{ortho}$ = 8.7 Hz, 2H), 7.28 (m, $J_{ortho}$ = 8.7 Hz, 2H), 6.01 (d, $J$ = 6.3 Hz, 1H), 5.88 (s, 1H), 4.61 (ddd, $J$ = 6.2 Hz, 4.7 Hz, 6.3 Hz, 1H), 4.15 (dd, $J$ = 4.7 Hz, 11.6 Hz, 1H), 4.15 (s, 2H), 4.00 (dd, $J$ = 6.2 Hz, 11.6 Hz, 1H), 3.72 (s, 2H). FDMS: *m/z* 610 ($M^+ + H$). HR-FABMS: calcd for $C_{23}H_{20}{}^{35}Cl_2F_3N_3O_9$ ($M^+ + H$) 610.0606, found 610.0605.

**Compound 13.** To a solution of **11** (78.2 mg, 0.168 mmol) in acetone (1.0 mL) was added 10% aqueous HCl (0.2 mL) at room temperature. After 1 h, the reaction mixture was diluted with water and the acetone was removed *in vacuo*. The mixture was extracted with EtOAc. The combined organic layers were washed with brine, dried over $MgSO_4$, filtered, concentrated *in vacuo*, and flash chromatographed (hexane/EtOAc = 1:2 and EtOAc) to give **13** as a colorless gum (30.7 mg, 48%). Compound **13** was purified by HPLC (YMC A-323: C-18 reverse-phase column, $\phi$ 10 mm × 250 mm, $CH_3CN$/0.1% aqueous TFA = 25:75, 3.0 mL/min, 278 nm) before use as a standard. The $CH_3CN$ and TFA were removed with a rotary evaporator, and the water was removed by lyophilization to give **13** as a colorless solid. $^1$H NMR (600 MHz, $CDCl_3$–$CD_3OD$): $\delta$ 8.20 (m, $J_{ortho}$ = 8.7 Hz, 2H), 7.56 (m, $J_{ortho}$ = 8.7 Hz, 2H), 5.80 (s, 1H), 5.07 (d, $J$ = 1.6 Hz, 1H), 4.50 (dd, $J$ = 6.1 Hz, 11.0 Hz, 1H), 4.42 (ddd, $J$ = 7.1 Hz, 6.1 Hz, 1.6 Hz, 1H), 4.35 (dd, $J$ = 7.1 Hz, 11.0 Hz, 1H), 4.20 (s, 2H). FDMS: *m/z* 381 ($M^+ + H$). HR-FABMS: calcd for $C_{13}H_{15}{}^{35}Cl_2N_2O_7$ ($M^+ + H$) 381.0256, found 381.0259.

To a solution of **5** (10.0 mg, 0.0163 mmol) in acetone (2.5 mL) was added 0.1 N aqueous NaOH (2.5 mL) at −13 °C. After 25 min, the reaction mixture was acidified with 1 N aqueous HCl and the acetone was removed *in vacuo*. The mixture was extracted with EtOAc. The combined organic layers were washed with brine, dried over $MgSO_4$, filtered, concentrated *in vacuo*, and flash chromatographed (EtOAc, EtOAc/*i*-PrOH/$H_2O$ = 10:2:0.1, and *i*-PrOH) to give **13** as a colorless gum (4.7 mg, 76%).

**Compound 14.** A solution of chloramphenicol (3.8766 g, 12.0 mmol), *tert*-butyldimethylsilyl chloride (1.8966 g, 12.6 mmol), and imidazole (1.6396 g, 24.1 mmol) in DMF (10 mL) was stirred at room temperature for 19 h. After the solvent was removed *in vacuo*, the residue was treated with saturated aqueous $NH_4Cl$ and the mixture was extracted with EtOAc. The combined organic layers were washed with brine, dried over $MgSO_4$, filtered, concentrated *in vacuo*, and flash chromatographed (hexane/EtOAc = 2:1) to give chloramphenicol monosilyl ether as a colorless gum (4.9946 g, 95%). To a solution of the silyl ether (519.0 mg, 1.186 mmol) in DMF (3.0 mL) was added NaH (60% in oil, 105.1 mg, 2.63 mmol) at 0 °C. After the reaction mixture was stirred for 10 min at room temperature and cooled to 0 °C, allyl bromide (123 $\mu$L, 1.42 mmol) was added. The reaction mixture was stirred at 0 °C for 1 h and at room temperature for 10.5 h, then the reaction was quenched with saturated aqueous $NH_4Cl$, and the mixture was extracted with EtOAc. The combined organic layers were washed with brine, dried over $MgSO_4$, filtered, concentrated *in vacuo*, and flash chromatographed (hexane/EtOAc = 4:1) to give **14** as a colorless gum (284.2 mg, 50%). $^1$H NMR (500 MHz, $CDCl_3$): $\delta$ 8.21 (d, $J$ = 8.6 Hz, 2H), 7.50 (d, $J$ = 8.6 Hz, 2H), 6.88 (d, $J$ = 9.1 Hz, 1H), 5.89 (m, 1H), 5.28–5.21 (m, 2H), 4.88 (d, $J$ = 3.5 Hz, 1H), 4.09 (m, 1H), 4.05 (m, 1H), 3.87 (m, 1H), 3.72 (dd, $J$ = 8.0 Hz, 9.6 Hz, 1H), 3.60 (dd, $J$ = 4.4 Hz, 9.6 Hz, 1H), 0.92 (s, 9H), 0.09 (s, 3H), 0.09 (s, 3H). FABMS: *m/z* 477 ($M^+$).

**Compound 15.** A solution of **14** (353.1 mg, 0.740 mmol) in acetic acid/THF/$H_2O$ (3:1:1, 3.0 mL) was stirred at room temperature for 3 days. The reaction mixture was concentrated *in vacuo* and flash chromatographed (hexane/EtOAc = 1:2) to give a colorless gum (218.4 mg, 68%). A solution of the gum (218.4 mg, 0.499 mmol), 4-((trifluoroacetyl)amino)phenylacetic acid (151.6 mg, 0.613 mmol), EDC (126.4 mg, 0.659 mmol), and 4-(dimethylamino)pyridine (DMAP) (7.8 mg, 0.064 mmol) in $CH_2Cl_2$ (15 mL) was stirred at room temperature for 11 h. The reaction mixture was concentrated *in vacuo* and flash chromatographed (hexane/EtOAc = 3:2) to give **15** as a colorless gum (315.2 mg, 100%). $^1$H NMR (500 MHz, $CDCl_3$–$CD_3OD$): $\delta$ 8.20 (d, $J$ = 8.4 Hz, 2H), 7.58 (d, $J$ = 8.4 Hz, 2H), 7.41 (d, $J$ = 8.4 Hz, 2H), 7.27 (d, $J$ = 8.4 Hz, 2H), 5.84 (m, 1H), 5.77 (s, 1H), 5.24 (d, $J$ = 9.7 Hz, 1H), 5.24 (d, $J$ = 17.7 Hz, 1H), 4.63 (s, 1H), 4.38–4.23 (m, 3H), 4.04 (dd, $J$ = 4.6 Hz, 12.5 Hz, 1H), 3.78 (dd, $J$ = 6.4 Hz, 12.5 Hz, 1H), 3.64 (s, 2H).

**Compound 6.** To a solution of **15** (315.2 mg, 0.592 mmol) and sodium periodate (1.1492 g, 5.373 mmol) in $CH_2Cl_2$ (2.0 mL)–$CH_3CN$ (2.0 mL)–$H_2O$ (1.6 mL)–acetic acid (1.6 mL) was added a solution of ruthenium(III) chloride hydrate (23.0 mg, 0.111 mmol) in $H_2O$ (1.5 mL) at room temperature. After 20 min, the reaction mixture was diluted with water and the volatile solvents were removed *in vacuo*. A 10% aqueous HCl (0.1 mL) solution was added, and the mixture was extracted with EtOAc. The combined organic layers were washed with brine, dried over $MgSO_4$, filtered, concentrated *in vacuo*, and flash chromatographed (EtOAc/*i*-PrOH/$H_2O$ = 9:1:0.4) to give **6** as a colorless gum (154.6 mg, 43%). The gum was purified by HPLC (YMC A-323: C-18 reverse-phase column, $\phi$ 10 mm × 250 mm, $CH_3CN$/0.1% aqueous TFA = 50:50, 3.0 mL/min, 278 nm) before use in the hydrolysis reaction. $CH_3CN$ and TFA were removed with a rotary evaporator, and the water was removed by lyophilization to give **6** as colorless solid. $^1$H NMR (600 MHz, $CDCl_3$–$CD_3OD$): $\delta$ 8.17 (m, $J_{ortho}$ = 8.3 Hz, 2H), 7.58 (m, $J_{ortho}$ = 8.3 Hz, 2H), 7.37 (m, $J_{ortho}$ = 8.3 Hz, 2H), 7.30 (m, $J_{ortho}$ = 8.3 Hz, 2H), 5.85 (s, 1H), 4.62 (d, $J$ = 4.1 Hz, 1H), 4.49 (dd, $J$ = 5.4 Hz, 11.4 Hz, 1H), 4.28 (ddd, $J$ = 6.1 Hz, 5.4 Hz, 4.1 Hz, 1H), 4.09 (dd, $J$ = 6.1 Hz, 11.4 Hz, 1H), 4.03 (d, $J$ = 16.8 Hz, 1H), 3.77 (d, $J$ = 16.8 Hz, 1H), 3.65 (s, 2H). FABMS: *m/z* 610 ($M^+ + H$). HR-FABMS: calcd for $C_{23}H_{21}{}^{35}Cl_2F_3N_3O_9$ ($M^+ + H$) 610.0606, found 610.0605.

**Compound 16.** To a solution of **15** (18.3 mg, 0.030 mmol) in MeOH (0.5 mL) was added 0.1 N aqueous NaOH (1.0 mL) at room temperature. After 30 min, the reaction mixture was acidified with 10% aqueous HCl and was purified by HPLC (YMC A-323: C-18 reverse-phase column, $\phi$ 10 mm × 250 mm, $CH_3CN$/0.1% aqueous TFA = 20:80, 3.0 mL/min, 278 nm) to give **16** as a colorless solid (9.37 mg, 82%). $^1$H NMR (600 MHz, $CDCl_3$–$CD_3OD$): $\delta$ 8.22 (d, $J$ = 8.6 Hz, 2H), 7.75 (d, 1H × 0.3), 7.53 (d, $J$ = 8.6 Hz, 2H), 4.99 (d, $J$ = 3.0 Hz, 1H), 4.22 (d, $J$ = 16.9 Hz, 1H), 4.13 (m, 1H), 3.90 (d, $J$ = 16.9 Hz, 1H), 3.87 (dd, $J$ = 7.2 Hz, 11.5 Hz, 1H), 3.74 (dd, $J$ = 4.4 Hz, 11.5 Hz, 1H). FDMS: *m/z* 381 ($M^+ + H$). HR-FABMS: calcd for $C_{13}H_{15}{}^{35}Cl_2N_2O_7$ ($M^+ + H$) 381.0256, found 381.0258.

**Compound 17.** A solution of **11** (259.2 mg, 0.557 mmol), 4-(acetylamino)phenylacetic acid (218.9 mg, 1.13 mmol), EDC (331.9 mg, 1.73 mmol), and DMAP (6.4 mg, 0.05 mmol) in $CH_2Cl_2$ (30 mL) was stirred at room temperature for 23 h. The reaction mixture was treated with saturated aqueous $NH_4Cl$, and the mixture was extracted with $CH_2Cl_2$. The combined organic layers were washed with brine, dried over $MgSO_4$, filtered, concentrated *in vacuo*, and flash chromatographed (hexane/EtOAc = 1:2) to give **17** as a colorless gum (235.0 mg, 66%). $^1$H NMR (600 MHz, $CDCl_3$): mixture of two isomers $\delta$ 8.17 (d, $J$ = 7.9 Hz, 2H), 7.50 (d, $J$ = 7.9 Hz, 2H), 7.36 (d, $J$ = 7.9 Hz, 2H), 7.23 (d, $J$ = 7.9 Hz, 2H), 7.15 (bs, 1H), 6.59 (bd, $J$ = 9.0 Hz, 1H), 6.04–6.02 (m, 1H), 5.77 (s, 1H), 4.72–4.67 (m, 1H), 4.60–4.54 (m, 1H), 4.22 (s, 2H × 0.5), 4.22 (s, 2H × 0.5), 4.28–4.14 (m, 1H), 4.07–3.99 (m, 1H), 3.88–3.81 (m, 1H), 3.69 (s, 2H), 3.55–3.51 (m, 1H), 2.19 (s, 3H), 1.88–1.25 (m, 6H). FDMS: *m/z* 639 ($M^+$).

**Compound 7.** To a solution of **17** (171.9 mg, 0.268 mmol) in acetone (1.0 mL) was added 10% aqueous HCl (0.1 mL) at room temperature. After 20 min, the reaction mixture was concentrated *in vacuo*. The residue was flash chromatographed (hexane/EtOAc = 1:2 and EtOAc) to give **7** as colorless gum (117.8 mg, 79%). The gum was crystallized from EtOAc to give **7** as colorless crystals. $^1$H NMR (500 MHz, $CDCl_3$–$CD_3OD$): $\delta$ 8.18 (m, $J_{ortho}$ = 8.3 Hz, 2H), 7.50

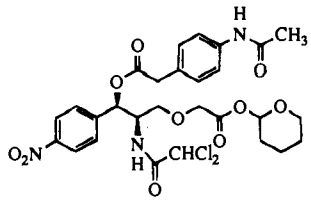

**17**

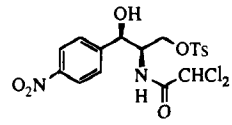

**18**

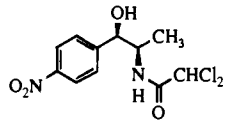

**19**

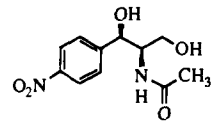

**20**

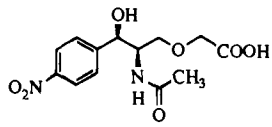

**21**

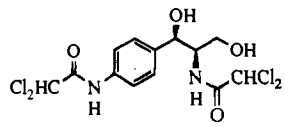

**22**

(m, $J_{ortho}$ = 8.3 Hz, 2H), 7.43 (m, $J_{ortho}$ = 8.3 Hz, 2H), 7.20 (d, $J$ = 8.3 Hz, 2H), 6.01 (d, $J$ = 6.0 Hz, 1H), 5.92 (s, 1H), 4.60 (ddd, $J$ = 6.2 Hz, 5.2 Hz, 6.0 Hz, 1H), 4.15 (dd, $J$ = 5.2 Hz, 11.5 Hz, 1H), 4.14 (s, 2H), 3.99 (dd, $J$ = 6.2 Hz, 11.5 Hz, 1H), 3.68 (s, 2H), 2.16 (s, 3H). FDMS: *m/z* 555 ($M^+$). HR-FABMS: calcd for $C_{23}H_{24}{}^{35}Cl_2N_3O_9$ ($M^+$ + H) 556.0890, found 556.0897.

**Compound 18.** A solution of chloramphenicol (1.2966 g, 4.01 mmol) and *p*-toluenesulfonyl chloride (881.2 mg, 4.62 mmol) in pyridine (10 mL) was stirred at room temperature for 2 h. The reaction mixture was acidified with 5% aqueous HCl and was extracted with EtOAc. The combined organic layers were washed with brine, dried over $MgSO_4$, filtered, concentrated *in vacuo*, and flash chromatographed (hexane/EtOAc = 1:1) to give **18** as a colorless solid (1.8616 g, 97%). $^1$H NMR (500 MHz, $CDCl_3$): $\delta$ 8.19 (d, $J$ = 8.7 Hz, 2H), 7.81 (d, $J$ = 8.2 Hz, 2H), 7.53 (d, $J$ = 8.7 Hz, 2H), 7.39 (d, $J$ = 8.2 Hz, 2H), 6.86 (d, $J$ = 8.6 Hz, 1H), 5.73 (s, 1H), 5.29 (d, $J$ = 2.1 Hz, 1H), 4.36 (m, 1H), 4.30 (dd, $J$ = 8.0 Hz, 10.2 Hz, 1H), 4.07 (dd, $J$ = 4.8 Hz, 10.2 Hz, 1H), 2.48 (s, 3H). FABMS: *m/z* 476 ($M^+$ + H).

**Compound 19.**[47] To a solution of **18** (94.5 mg, 0.198 mmol) in THF (2.0 mL) was added $LiAlH_4$ (73.3 mg, 1.93 mmol) at 0 °C. After the reaction mixture was stirred 0 °C for 20 min and at room temperature for 2 h, the reaction was quenched with ice-cold 2% aqueous HCl and the mixture was extracted with EtOAc. The combined organic layers were washed with brine, dried over $MgSO_4$, filtered, concentrated *in vacuo*, and flash chromatographed (hexane/EtOAc = 1:1) to give **19** as a colorless gum (10.3 mg, 17%). $^1$H NMR (600 MHz, $CDCl_3$): $\delta$ 8.20 (m, $J_{ortho}$ = 8.9 Hz, 2H), 7.54 (m, $J_{ortho}$ = 8.9 Hz, 2H), 6.70 (bd, $J$ = 8.1 Hz, 1H), 5.79 (s, 1H), 4.92 (d, $J$ = 3.4 Hz, 1H), 4.25 (m, 1H), 1.34 (d, $J$ = 6.9 Hz, 3H), FABMS: *m/z* 307 ($M^+$ + H). HR-FABMS: calcd for $C_{11}H_{13}Cl_2N_2O_4$ ($M^+$ + H) 307.0252, found 307.0254.

**Compound 8.** A solution of **19** (27.7 mg, 0.0902 mmol), 4-((trifluoroacetyl)amino)phenylacetic acid (28.6 mg, 0.116 mmol), EDC (24.6 mg, 0.128 mmol), and DMAP (2.6 mg, 0.02 mmol) in $CH_2Cl_2$ (5.0 mL) was stirred at room temperature for 4.5 h. The reaction mixture was concentrated *in vacuo* and flash chromatographed (hexane/EtOAc = 1:1) to give **8** as a colorless gum (35.6 mg, 74%). The gum was crystallized from $CH_2Cl_2$–MeOH to give **8** as colorless crystals. $^1$H NMR (500 MHz, $CDCl_3$–$CD_3OD$): $\delta$ 8.20 (m, $J_{ortho}$ = 8.6 Hz, 2H), 7.62 (m, $J_{ortho}$ = 8.6 Hz, 2H), 7.42 (m, $J_{ortho}$ = 8.6 Hz, 2H), 7.29 (m, $J_{ortho}$ = 8.6 Hz, 2H), 6.92 (d, $J$ = 9.3 Hz, 1H × 0.5), 5.82 (d, $J$ = 8.2 Hz, 1H), 5.81 (s, 1H), 4.40 (m, 1H), 3.72 (s, 2H), 1.12 (d, $J$ = 7.0 Hz, 3H). FABMS: *m/z* 536 ($M^+$ + H). HR-FABMS: calcd for $C_{21}H_{19}{}^{35}Cl_2F_3N_3O_6$ ($M^+$ + H) 536.0603, found 536.0597.

**Compound 20.**[48] Acetic anhydride (6.5 mL, 68.9 mmol) was added to D-*threo*-2-amino-1-(4-nitrophenyl)-1,3-propanediol (2.5409 g, 12.0 mmol) at room temperture. After the mixture was stirred at room temperature for 2 h, crystals were generated and the mixture was filtered. The crystals were collected and washed with EtOAc to give **20**, as colorless crystals (1.5358 g, 50%). $^1$H NMR (500 MHz, $CDCl_3$–$CD_3OD$): $\delta$ 8.20 (m, $J_{ortho}$ = 8.7 Hz, 2H), 7.57 (m, $J_{ortho}$ = 8.7 Hz, 2H), 5.81 (bd, $J$ = 8.8 Hz, 1H × 0.5), 5.14 (d, $J$ = 2.4 Hz, 1H), 4.05 (m, 1H), 3.69–3.63 (m, 2H), 1.88 (s, 3H). FABMS: *m/z* 255 ($M^+$ + H). HR-FABMS: calcd for $C_{11}H_{15}N_2O_5$ ($M^+$ + H) 255.0981, found 255.0979.

**Compound 9.** Sodium hexamethyldisilazide (1 M in THF, 2.1 mL, 2.10 mmol) was added to a solution of **20** (508.9 mg, 2.00 mmol) in DMF (2.0 mL) at −45 °C and was followed after 30 min by the addition of allyl bromide (207 $\mu$L, 2.40 mmol). The reaction mixture was allowed to warm to room temperature over a 5 h period and was stirred at room temperature for 11 h. The reaction was quenched with 1% aqueous HCl, and the mixture was extracted with EtOAc. The combined organic layers were washed with brine, dried over $MgSO_4$, filtered, concentrated *in vacuo*, flash chromatographed (EtOAc), and purified by preparative TLC (EtOAc) to give the allyl ether as a colorless gum (89.5 mg, 15%). A solution of the allyl ether (46.0 mg, 0.156 mmol), 4-((trifluoroacetyl)amino)phenylacetic acid (43.5 mg, 0.183 mmol), EDC (64.3 mg, 0.335 mmol), and DMAP (1.0 mg, 0.008 mmol) in $CH_2Cl_2$ (2.5 mL) was stirred at room temperature for 18 h. The reaction mixture was concentrated *in vacuo* and purified by preparative TLC (hexane/EtOAC = 1:2) to give the ester as a colorless gum (37.3 mg, 51%). To a solution of the ester (105.2 mg, 0.227 mmol) and sodium periodate (440.3 mg, 2.06 mmol) in $CH_2Cl_2$ (1.0 mL)–$CH_3CN$ (1.0 mL)–$H_2O$ (0.8 mL)–acetic acid (0.8 mL) was added a solution of ruthenium(III) chloride hydrate (10.3 mg, 0.497 mmol) in $H_2O$ (0.8 mL) at room temperature. After 2 h, the reaction mixture was diluted with water and 10% aqueous HCl (0.1 mL) and the mixture was extracted with EtOAc. The combined organic layers were washed with brine, dried over $MgSO_4$, filtered, concentrated *in vacuo*, and flash chromatographed (EtOAc/*i*-PrOH/$H_2O$ = 9:1:0.4) to give **9** as a colorless gum (39.1 mg, 32%). The gum was crystallized from EtOAc to give **9** as colorless crystals. $^1$H NMR (500 MHz, $CDCl_3$–$CD_3OD$): $\delta$ 8.21 (m, $J_{ortho}$ = 8.4 Hz, 2H), 7.59 (m, $J_{ortho}$ = 8.4 Hz, 2H), 7.56 (m, $J_{ortho}$ = 8.6 Hz, 2H), 7.29 (m, $J_{ortho}$ = 8.6 Hz, 2H), 6.04 (d, $J$ = 8.7 Hz, 1H), 4.43 (ddd, $J$ = 2.3 Hz, 3.1 Hz, 8.7 Hz, 1H), 3.92 (AB, $J$ = 16.6 Hz, $\Delta\nu$ = 34.6 Hz, 2H), 3.64 (AB, $J$ = 14.7 Hz, $\Delta\nu$ = 15.9 Hz, 2H), 3.35 (dd, $J$ = 3.1 Hz, 9.6 Hz, 1H), 3.20 (dd, $J$ = 2.3 Hz, 9.6 Hz, 1H), 1.80 (s, 3H). FABMS: *m/z* 540 ($M^+$ − H). HR-FABMS: calcd for $C_{23}H_{21}F_3N_3O_9$ ($M^+$ − H) 540.1230, found 540.1223.

**Compound 21.** NaH (60% in oil, 50.0 mg, 1.25 mmol) was added to a solution of **20** (201.1 mg, 0.791 mmol) in THF (2.5 mL) at 0 °C, and after 40 min, a solution of (tetrahydropyranyl)iodoacetic acid (234 mg, 0.866 mmol) was added. The reaction mixture was stirred at 0 °C for 1 h and then stirred at room temperature for 10 h. The reaction was quenched with saturated aqueous $NH_4Cl$, and the reaction mixture was extracted with EtOAc. The combined organic layers were washed with brine, dried over $MgSO_4$, filtered, concentrated *in vacuo*, and purified by preparative TLC (hexane/EtOAc = 1:2) to give a colorless gum (98.4 mg, 31%). To a solution of the gum (57.6 mg, 0.145 mmol) in acetone (0.5 mL) was added 10% aqueous HCl (0.05 mL) at room temperature. After 1 h, the reaction mixture was purified by preparative TLC (EtOAc) to give **21** as a colorless gum (17.0 mg, 37%). The gum was crystallized from $CHCl_3$–MeOH to give **21** as colorless crystals. $^1$H NMR (600 MHz, $CDCl_3$–$CD_3OD$): $\delta$ 8.20 (m, $J_{ortho}$ = 8.6 Hz, 2H), 7.56 (m, $J_{ortho}$ = 8.6 Hz, 2H), 4.98 (m, 1H), 4.41 (m, 1H), 4.39 (m, 1H), 4.22 (m, 1H), 4.17 (s, 2H), 1.87 (s, 3H). FABMS: *m/z* 313 ($M^+$ + H). HR-FABMS: calcd for $C_{13}H_{17}N_2O_7$ ($M^+$ + H) 313.1035, found 313.1044.

**Compound 22.** A mixture of D-*threo*-2-amino-1-(4-nitrophenyl)-1,3-propanediol (1.0108 g, 4.76 mmol) and platinum(IV) oxide (24.3 mg, 0.107 mmol) in EtOH (25 mL)–$H_2O$ (5 mL) was stirred at room temperature for 10 h under $H_2$. The mixture was filtered. The filtrate was concentrated *in vacuo* to give a colorless residue. To the residue

(47) Cullis, P. M.; Lewendon, A.; Shaw, W. V.; Williams, J. A. *Biochemistry* **1991**, *30*, 3758.

(48) Rebstock, M. C.; Crook, H. M. J.; Controulis, J.; Bartz, Q. R. *J. Am. Chem. Soc.* **1949**, *71*, 2458.

**Table 4.** Retention Times of Substrates and Hydrolyzed Products in HPLC Assays[a]

| substrate/ product | retention time (min) (substrate/product) | elution ($CH_3CN$/0.1% aqueous TFA) |
|---|---|---|
| **5/13** | 11.8/4.5 | 50:50 |
| **6/16** | 13.9/4.5 | 50:50 |
| **7/13** | 5.6/4.5 | 50:50 |
| **8/19** | 15.2/5.6 | 55:45 |
| **9/21** | 13.9/3.9 | 40:60 |
| **10/22**[b] | 12.0/4.4 | 50:50 |

[a] HPLC assays were performed using a YMC ODS A303 column at flow rate of 1.0 mL/min at 278 nm. [b] Isomerization of the ester group of substrate **10** between C-1 and C-3 exists during the assay. The retention time of the regioisomer of **10** was 14.5 min in the assay of **10/22**.

was added dichloroacetic anhydride (3.04 mL, 19.9 mmol) at room temperature. After 12 h, ice and solid $NaHCO_3$ were added and the mixture was extracted with EtOAc. The combined organic layers were washed with brine, dried over $MgSO_4$, filtered, and concentrated *in vacuo*, to give a colorless residue. The residue was dissolved in MeOH (30 mL), and then, 0.1 N aquoeus NaOH (50 mL) was added at room temperature. After 10 min, the reaction mixture was acidified with 10% aqueous HCl and the MeOH was removed *in vacuo*. The mixture was extracted with EtOAc. The combined organic layers were washed with brine, dried over $MgSO_4$, filtered, concentrated *in vacuo*, flash chromatographed (EtOAc), and crystallized from EtOAc to give **22** as colorless crystals (1.6866 g, 88% from D-*threo*-2-amino-1-(4-nitrophenyl)-1,3-propanediol). $^1H$ NMR (500 MHz, $CDCl_3$–$CD_3OD$): $\delta$ 7.54 (m, $J_{ortho}$ = 8.5 Hz, 2H), 7.37 (m, $J_{ortho}$ = 8.5 Hz, 2H), 6.14 (s, 1H), 5.91 (s, 1H), 5.07 (d, $J$ = 3.0 Hz, 1H), 4.04 (m, 1H), 3.77 (dd, $J$ = 6.2 Hz, 11.2 Hz, 1H), 3.73 (dd, $J$ = 4.7 Hz, 11.2 Hz, 1H). FABMS: $m/z$ 405 ($M^+$ + H). HR-FABMS: calcd for $C_{13}H_{15}{}^{35}Cl_4N_2O_4$ ($M^+$ + H) 402.9786, found 402.9773.

**Compound 10.** A solution of **22** (1.0042 g, 2.485 mmol), *tert*-butyldimethylsilyl chloride (414.5 mg, 2.75 mmol), and imidazole (381.9 g, 5.61 mmol) in DMF (10 mL) was stirred at room temperature for 3 h. The solvent was removed *in vacuo*, treated with saturated aqueous $NH_4Cl$, and extracted with EtOAc. The combined organic layers were washed with brine, dried over $MgSO_4$, filtered, and concentrated *in vacuo* to give a colorless residue. A solution of the residue, 4-((trifluoroacetyl)amino)phenylacetic acid (852.7 mg, 3.45 mmol), EDC (992.4 mg, 5.18 mmol), and DMAP (17.4 mg, 0.142 mmol) in $CH_2Cl_2$ (18 mL) was stirred at room temperature for 7 days. The reaction mixture was treated with saturated aqueous $NH_4Cl$, and the mixture was extracted with $CH_2Cl_2$. The combined organic layers were washed with brine, dried over $MgSO_4$, filtered, concentrated *in vacuo*, and flash chromatographed (hexane/EtOAc = 1:1) to give a colorless gum (1.4391 g). The gum was dissolved in acetic acid/THF/$H_2O$ (3:1:1, 20 mL), and the mixture was stirred at room temperature for 15 h. The reaction mixture was concentrated *in vacuo* and crystallized from hexane–EtOAc to give **10** as colorless crystals (309.8 mg, 20% from **22**). The mother liquor was concentrated *in vacuo* and flash chromatographed (hexane/EtOAc = 1:2) to give **10** as a colorless solid (423.9 mg, 27% from **22**). $^1H$ NMR (600 MHz, $CDCl_3$–$CD_3OD$): $\delta$ 7.56 (d, $J$ = 8.3 Hz, 2H), 7.54 (d, $J$ = 8.3 Hz, 2H), 7.28 (d, $J$ = 8.3 Hz, 2H), 7.23 (d, $J$ = 8.3 Hz, 2H), 6.14 (s, 1H), 5.98 (d, $J$ = 8.0 Hz, 1H), 5.93 (s, 1H), 4.23 (m, 1H), 3.64 (AB, $J$ = 15.3 Hz, $\Delta\nu$ = 11.3 Hz, 2H), 3.52 (dd, $J$ = 4.1 Hz, 11.5 Hz, 1H), 3.36 (dd, $J$ = 4.1 Hz, 11.5 Hz, 1H). FABMS: $m/z$ 634 ($M^+$ + H). HR-FABMS: calcd for $C_{23}H_{21}{}^{35}Cl_4F_3N_3O_6$ ($M^+$ + H) 632.0136, found 632.0126.

**Catalytic Assays and Kinetic Measurements.** Reactions were initiated by adding 10 $\mu$L of a stock solution of substrate in DMSO to 90 $\mu$L of antibody solution in 50 mM Tris, pH 8.0 at 25 °C, unless otherwise noted. Hydrolysis rates were measured by HPLC detection of the products with 10 $\mu$L injection of the reaction mixture. The analytical HPLC was performed on a Waters 600 unit equipped with a Waters 490 multiwavelength detector, using a YMC ODS A303 column eluted with $CH_3CN$/0.1% aqueous TFA at a flow rate of 1.0 mL/min, with detection at 278 nm. The retention times of the substrates and the products are shown in Table 4. Initial rates were determined from the linear range of the rate. The observed rate was corrected of the uncatalyzed rate of hydrolysis in the absence of antibody. The kinetic parameters, $k_{cat}$ and $K_m$, were determined by a linear least-squares fitting of the Lineweaver–Burk plots described by the Michaelis–Menten equation. The rate constants, $k_{cat}$'s, were obtained by dividing by the concentration of antibody-combining sites (2 × [IgG]). Background rates ($k_{uncat}$) were determined in the absence of antibody under otherwise identical conditions. The inhibition constant, $K_i$, was extrapolated from the Dixon plots.

**Binding Assays (CIEIA).** Microtiter plates (96-well flat-bottom Coster ELISA plates) were coated with transition state analog **3**–BSA conjugate (50 $\mu$L, 10 $\mu$g/mL in 20 mM PBS, pH 7.4) for 2 h at room temperture, washed with PBS, blocked with gelatin (300 $\mu$L, 1% in 10 mM sodium phosphate buffer, 0.02% $NaN_3$, pH 7.4) for 18 h at room temperature, and stored at 4 °C. The plates were washed with PBS, and CIEIA were performed. Piror to carrying out the CIEIA, the optimum antibody concentrations were determined by ELISA to establish a reproducible titration curve (the sigmoidal plot of the log of the antibody concentration vs absorbance). The antibody concentration was definded as the concentration at which OD < 1.0 and which >70% of the antibody binds to the **3**–BSA conjugate. CIEIA were performed as follows. To a 45 $\mu$L solution of antibody in PBS per well of the **3**–BSA conjugate coated plate was added a 5 $\mu$L solution of each inhibitor (transition state analog **3** or substrate **5**) in DMSO at room temperature. After 1 h, the plate was washed with PBS and the ELISA was performed using the Vectastain Elite ABC kit (biotinylated anti-mouse IgG, avidin DH, and biotinylated horseradish peroxidase) (Vector Laboratories) and the peroxidase substrate kit [2,2′-azinobis-(3-ethylbenzothiazoline-6-sulfonic acid) and hydrogen peroxide] (Bio-Rad). Dissociation constants ($K_S$ and $K_{TSA}$) were determined as the inhibitor concentration required to inhibit 50% of the maximal binding in a titration cuve (the sigmoidal plot of the log of the inhibitor concentration vs inhibition percentage to the maximal binding) of CIEIA. Each dissociation constant was determined in triplicate, and the average of the three determinations was used as the final value. The $K_S/K_{TSA}$ value was calculated as the ratio of the dissociation constant for substrate **5** relative to that for the transition state analog **3**.

**Chemical Modification of Antibodies.** Hydrolytic activities of the modified antibodies were assayed using 1.0 $\mu$M of modified antibody and 100 $\mu$M of substrate **5**.

(a) Arginine. A 50 $\mu$L aliquot of a 6 mM phenylglyoxal solution in 125 mM $NaHCO_3$ (pH 8.3) was added to buffer (195 $\mu$L, 125 mM $NaHCO_3$, pH 8.3) containing 10 $\mu$M antibody. The solution was incubated at room temperature overnight. The buffer was then exchanged to 50 mM sodium phosphate buffer (pH 7.5) using a Centricon-30 unit (Amicon). Protein concentrations were determined by BCA protein assay (Pierce), and assays were performed for catalytic activity. (b) Tyrosine. A 1 $\mu$L aliquot of a 200 mM tetranitromethane solution in dioxane was added to a 20 $\mu$M antibody solution (100 $\mu$L) in 50 mM Tris buffer (pH 8.0). The solution was incubated for 1 h at room temperature, and then, the buffer was exchanged to 50 mM sodium phosphate buffer (pH 7.5) by gel filtration (PD-10 Pharmacia). Protein concentrations were determined by BCA. (c) Histidine. A 1 $\mu$L aliquot of a 25 mM diethyl pyrocarbonate solution was added to a 10 $\mu$M antibody solution (50 $\mu$L) in 50 mM sodium phosphate buffer (pH 7.0). The solution was incubated for 1 h at room temperature. The buffer was then exchanged to 50 mM sodium phosphate buffer (pH 7.5) using a Centricon-30 unit (Amicon), and the protein concentrations were determined by BCA. (d) Reactivation of DEPC-modified antibody 6D9 with hydroxylamine. A solution of 5.0 $\mu$M DEPC-modified antibody 6D9 (with <2% original activity) and 25 mM hydroxylamine in 50 mM sodium phosphate buffer (pH 7.0) was made by the addition of 2.5 M hydroxylamine. After incubation at 25 °C for 15 min, the hydrolytic activity was compared to controls of identically treated, native catalytic antibody 6D9. This concentration of hydroxylamine neither affected the antibody stability nor interfered with the assay.

**pH Profiles.** The variation of $k_{cat}$ as a function of pH was determined between pH 8.0 and 8.5 in ATE buffer (100 mM ACE, 52 mM Tris, 52 mM ethanolamine) and between pH 6.0 and 8.0 in 50 mM sodium phosphate buffer. Reactions were initiated by adding 10 $\mu$L of a stock solution of substrate **5** in DMSO to 90 $\mu$L of antibody solution in the

indicated buffer at 25 °C. Hydrolysis rates were measured by HPLC detection according to the same method described in Catalytic Assay and Kinetic Measurements. The observed rate was corrected for the uncatalyzed rate of hydrolysis in the absence of antibody. The kinetic parameters, $k_{cat}$ and $K_m$, were determined by a linear least-squares fitting of the Lineweaver–Burk plots described by the Michaelis–Menten equation. The rate constants, $k_{cat}$'s, were obtained by dividing by the concentration of antibody-combining sites (2 × [IgG]). Background rates ($k_{uncat}$) were determined in the absence of antibody under otherwise identical conditions. The $k_{cat}$'s and $k_{uncat}$'s at pH 8.0 were not identical in the both buffer systems (ATE and sodium phosphate buffer).

**Modeling.** The coordinates of $V_H$ and $V_L$ of the murine anti-peptide antibody B13I2 were used for the parent structure.[36] The canonical structures of L1~3 and H1 of 6D9 are identical to those of B13I2. The modeling strategy of 6D9 is as follows: (1) model the H2 and H3 loops, (2) replace the loops of the parent molecule with the modeled loops, (3) replace the nonconserved side chains with those of 6D9, (4) minimize the energy.

The H2 loop was constructed from H2 of the crystal structure of antibody HIL (PDB code 1HIL), according to the canonical structure class. Crystal structures of known H3 loops do not have obvious canonical forms and vary greatly in length and conformation. In the case of the H3 loop, H3 of antibody R19.9 (PDB code 1FAI) was selected on the basis of the length and the amino acid sequence homology. The length of H3 of 6D9 is one residue shorter than that of R19.9. Therefore the central residue of H3 of R19.9 was excised, and the structure of the five residues in the midregion of the loop was reconstructed using the program CONGEN.[49]

The modeled loops were grafted onto the parent framework structure by superimposing the backbone atoms (N, C, and Cα) of the three residues preceding and the three residues following the loop onto the corresponding atoms of the parent molecule.

The initial conformations of the nonconserved side chain were traced according to the corresponding $\chi$ angles of the parent molecule as possible as we could. The untraceable side chains were initially created by using the rotamer library defined by Ponder and Richards.[50] The side chain conformations were optimized by the deadend algorithm with the "large-size" rotamer library.[51–53] After the joint regions of loops were energy minimized, the whole structure was minimized with positional restraints on Cα atoms in framework by program PRESTO.[54] The hapten was docked with the modeled combining site manually on the basis of the information from the substrate specificity of antibody 6D9.

JA944180M

(49) Bruccoleri, R. E.; Karplus, M. *Biopolymers* **1987**, *26*, 137.
(50) Ponder, J. W.; Richards, F. M. *J. Mol. Biol.* **1987**, *193*, 775.
(51) Tanimura, R.; Kidera, A.; Nakamura, H. *Protein Sci.* **1994**, *3*, 2358.
(52) Desmet, J.; De Maeyer, M.; Hazes, B.; Lasters, I. *Nature* **1992**, *356*, 539.
(53) Lasters, I.; Desmet, J. *Protein Eng.* **1993**, *6*, 717.
(54) Morikami, K.; Nakai, T.; Kidera, A.; Saito, M.; Nakamura, H. *Comput. Chem.* **1992**, *16*, 243.